RESULTS AND DISCUSSION

CHAPTER IV

RESULTS AND DISCUSSION

Introduction:

The process of alpha decay in nuclei has traditionally been assumed to be governed by the many characteristic properties (Coulomb barrier, spin, parity, etc.) of the parent isotope and the alpha particle. This implies that each pair of parent–daughter transition is only marginally related to other pairs of the same element.

4.1 Characteristics of alpha decay of even-even nuclei:

Fig. 4.1 shows the potential barrier provided by the parent and the daughter nuclei for the alpha decay of the parent nucleus ^{230}Th with the Q- value of the reaction 4.77 MeV. Here the potential for the overlapping region from parent nucleus radius to the touching configuration radius is calculated using the second order polynomial of Eq. (3.12) mentioned in chapter III. The potential from touching configuration to the point R_b of the Eq.(3.11) is calculated using the proximity and the coulomb potential of Eq. (3.13). Calculated characteristic quantities for 34 even-even nuclei with $208 \leq A \leq 288$ are presented in table 4.1. The Q-values for these nuclei varies from 4.573 to 9.975 MeV. The assault frequencies calculated using eq. (3.6) is of the order of the order of 10^{21} /s.

Fig. 4.2 represents the calculated preformation probabilities of the 34 even-even nuclei calculated using Eq. (3.9). Here the preformation probability is calculated using WKB penetrability which is considered to be the probability for the potential of overlapping region using the idea of Poenaru et al [48] [49]. Minimum value of ~~0.2826~~ 0.2382 which corresponds to the parent neutron number 150, which is nearer the magic number of 152 in the heavy region. Near the neutron number 126 among the calculated nuclei, for the parent neutron number N=124, the value of preformation probability is 0.3493 and near parent neutron number N=152, for N=150 the value of preformation probability is formed to be 0.2382.

Fig. 4.3 presents the calculated $\log_{10}$ P with respect to parent neutron number, N. Also total penetrability is calculated using the Eq.(3.8), since the values are very small values, so it is represented using logarithmic scale. In fig.4.3 log P is presented for 34 Even-even nuclei. Minimum value of -28.833 is found for the parent nuclei with N=124. The second lowest value -37.649 occur for N=150. Fig.4.4 clearly shows two fitting lines belonging to two regions and neutron magic number i.e. N=128 and N=152. Geiger-Nuttal rule is verified through our calculation. In fig 4.4 (a) the corresponding equation of straight line is given by $\log_{10}T_{1/2}=141.95Q^{-1/2}-52.737$. Similarly in fig.4.4 (b) shows two fitting line corresponding to parent neutron N=126 region and N=152. The respective straight line equation for the fitting line is given by $\log_{10}T_{1/2}=115.53Q^{-1/2}-38.262$. For the super heavy nuclei $^{270}_{108}$H, $^{288}_{114}$Fl. Calculations was made and better matching is found between calculated and experimental half-life for the nuclei $^{270}_{108}$Hs. Experimental half-life are taken from [50]. Better matching between calculated and experimental half-lives is formed for most of the considered nuclei except for a few systems. Fig.4.5 shows a single universal curve for alpha decay, similar to the one obtained by Poenaru et al [51]. In the case of even-even nuclei for 31 nuclei the standard deviation is found to be 0.632.

4.2 Characteristics of alpha decay of even-odd nuclei:

Fig.4.6 represents the potential barrier provided by the parent and the daughter nuclei for the alpha decay for the parent nucleus ^{210}Bi with the Q-value of the reaction 5.036 MeV. By using the second order polynomial of the form of Eq. (3.12) mentioned in chapter III the potential for the overlapping region from the parent nucleus radius to the toughing configuration radius is calculated. Potential from the touching configuration to the point R_b of the Eq. (3.11) is calculated using the proximity and coulomb potential of Eq. (3.13). Table 4.2 contains the calculated characteristics quantities for 40 even-odd nuclei with $210 \leq A \leq 290$. The Q value for these nuclei ranges from 5.036 to 11.605 MeV. By using Eq. (3.6) the assault frequencies are found which is of the order of 10^{21}/s

Fig.4.7 shows the calculated Preformation probabilities of the 40 even-odd nuclei which are calculated by using the Eq. (3.9). The WKB penetrability is used to calculate the preformation probability. From Fig.4.7 the minimum value for parent neutron number 155 is 0.263 and its corresponding daughter neutron number is 153, which is nearer the magic number 152 in the heavy region. Near the neutron number 126, among the calculated nucleus, for the parent neutron number N=127, the value of preformation probability is 0.349 and near the parent neutron number N=152, for N=150, the value of Preformation probability is formed to be 0.263.

Fig.4.8 is obtained by taking the calculated log P values with respect to parent neutron number N for the even odd nuclei. The total penetrating probability is calculated by using the Eq. (3.8). Since the values are very small the corresponding logarithmic scale values were found. In fig 4.8 log P is presented for 40 even-odd nuclei. The minimum value of –28.414 is obtained for N=155, similarly the second lowest value is -29.282 for N=127. Fig 4.9(a), (b) clearly denotes that there is two fitting lines that corresponds to two magic numbers N=126 and N=152. Through our calculation the Geiger-Nuttal is verified. Finally the equation of straight line for this fig is given by $\log_{10}T_{1/2}=125.51Q^{-1/2}-46.758$. Fig.4.9 (b) represents clearly represents the two fitting lines which belongs two regions of neutron numbers i.e. N=126 and N=152 in which the equation of straight line is given by $\log_{10}T_{1/2}=129.86Q^{-1/2}-42.468$. Calculations include for 19 super heavy nuclei they are $^{260}_{107}$Bh , $^{260}_{107}$Bh, $^{266}_{109}$Sg, $^{268}_{109}$Sg, $^{270}_{107}$Bh, $^{270}_{109}$Sg, $^{272}_{107}$Bh, $^{272}_{111}$Rg, $^{276}_{109}$Sg, $^{278}_{109}$Sg, $^{278}_{111}$Rg, $^{280}_{111}$Rg, $^{282}_{111}$Rg, $^{284}_{113}$Ed, $^{286}_{113}$Ed, $^{288}_{115}$Ef, $^{290}_{115}$Ef. In the case of even-odd nuclei for 22 nuclei the standard deviation is found to be 0.520. Fig 4.10 (a) and fig 4.10 (b) represents a representation for the universal curve as obtained by Poenaru et al [51].

4.3 Characteristics of odd-even nuclei:

Fig. 4.11 shows the potential barrier provided by the parent and the daughter nuclei for the alpha decay of the parent nucleus ^{235}U with the Q- value of the reaction 4.678 MeV. Here the second order polynomial of Eq. (3.12) mentioned in chapter III is used to calculate the potential for the overlapping region from parent nucleus radius to the touching configuration radius. The potential from touching configuration to the point R_b of the Eq. (3.11) is calculated using the proximity and the coulomb potential of Eq. (3.13). For 47 odd-even nuclei with $208 \leq A \leq 294$ the calculated characteristic quantities are presented in table 4.3. The Q-values for these nuclei varies from 4.678 to 12.275 MeV. Using Eq. (3.6) assault frequencies is calculated which is of the order of the order of 10^{21} /s.

Fig. 4.12 represents the calculated preformation probabilities for the 47 odd-even nuclei calculated using Eq. (3.9). Minimum value of 0.245 which corresponds to the parent neutron number 151, the daughter neutron number is 149, which is nearer the magic number of 152 in the heavy region. Near the neutron number 126 among the calculated nucleus, for the parent neutron number N=125, the value of preformation probability 0.416 and near parent neutron number N=152, for N=150 the value of preformation probability is formed to be 0.245

In fig. 4.13 calculated $\log_{10} P$ is drawn with respect to parent neutron number N for 47 odd-even nuclei. Minimum value of -20.727 is found for the parent nuclei with N=125. The second lowest value 12.275 occur for N=151. Here both these neutron number are nearer to the magic numbers 126 and 152. Fig 4.14 (a), (b) clearly denotes that there is two fitting lines that corresponds to two magic numbers N=126 and N=152. Through our calculation the Geiger-Nuttal is verified. Finally the equation of straight line for this fig is given by $\log_{10}T_{1/2}=155.88Q^{-1/2}-57.921$. Similarly fig. 4.15 shows two fitting lines corresponding to parent neutron N=126 and N=152. The respective straight line equation for the fitting line is given by $\log_{10}T_{1/2}=119.74Q^{-1/2}-39.599$. Here the

calculations include 17 super heavy nuclei with $104 \leq Z \leq 114$. They are $^{255}_{104}$Rf, $^{257}_{100}$Fm, $^{257}_{104}$Rf, $^{265}_{108}$Hs, $^{267}_{110}$Ds, $^{269}_{108}$Hs, $^{296}_{110}$Ds, $^{271}_{110}$Ds, $^{273}_{110}$Ds, $^{275}_{108}$Hs, $^{277}_{112}$Cn, $^{281}_{110}$Ds, $^{281}_{112}$Cn, $^{285}_{112}$Cn, $^{285}_{114}$Fl, $^{287}_{114}$Fl, $^{289}_{114}$Fl. In the case of odd- even nuclei for24 nuclei, the standard deviation is found to be 0.768. In fig 4.15 (a) and fig 4.15(b) represents a representation for the universal curve as obtained by Poenaru et al [51]

4.4 Dynamical cluster decay model:

The dynamical cluster decay model is developed for the decay of hot and rotating compound nuclei (CN) formed in light heavy reactions. The model is worked out in terms of only one parameter, namely the neck-length parameter, which is related to the total kinetic energy TKE (T) or effective Q value $Q_{eff}(T)$ at the temperature T of the hot CN and is defined in terms of the CN binding energy and ground-state binding energies of the emitted fragments.

De-excitation of hot and rotating ^{48}Cr formed in ^{24}Mg+^{24}Mg reaction:

Fully energy damped cross sections of the ^{24}Mg+^{24}Mg reaction at E_{cm}=44.4 MeV was studied by Hasan et al [51]. De-excitation of hot and rotating ^{48}Cr* compound nucleus formed in this reaction is studied using dynamical cluster-decay model (DCM) of Gupta and Collaborators [8]. The methodology is explained in chapter III. The calculations and the results are discussed in the following sections.

4.5 Fragmentation potential:

Fig.4.16 represents the fragmentation potential as a function of mass number A_2 for the decay of ^{48}Cr* formed in ^{24}Mg+^{24}Mg reaction for all change minimized binary fragments of the outgoing channel. This is calculated using eq. (3.26) mentioned in chapter III. This calculation is for the temperature t=0 MeV and at R=$R_t$fm and angular momentum $\ell=0\hbar$. Here the binding energy is due to Guet at al [47]. Even though there is no explicit preference for four nucleon structure, there is minima noted for ^{4}He and ^{16}O

and a slight odd-even structure is noted for other fragments. However this does not enter in the calculation. It is to be mentioned here that no fitting of parameters is carried out for fitting the binding energies due to Guet et al [47] with the experimental binding energies of Audi et al [42].

Temperature dependent fragmentation potential as a function of mass number A_2 is drawn in fig. 4.17 for a different angular momentum values ℓ=0 $\hbar$ to 50 $\hbar$. It is calculated at T=3.43 MeV with R=R_t+1 fm. Here there is not preference for alpha structure nuclei. However, as the angular momentum increases from 0 to 50 $\hbar$ symmetric channel is preferred, whereas at lower angular momentum, light particle is preferred. Cross section is the combined effect of preformation probability and penetration probability. Penetration probability contributes to the total cross sections from ℓ=0 $\hbar$ onwards. Above 10 $\hbar$ the value of penetration probability increases steeply with ℓ.

Fig.4.18 shows the fragmentation probabilities as a function of angular momentum ($\ell\hbar$). For both light particles ($A_2 \leq 4$), and intermediate mass fragments (A_2<4) the free parameter ΔR is varied by 1 fm. Here no attempt is made to vary ΔR such that calculated cross sections exactly fit with the experimental mass fragments. In fig.4.18, P_0 is high for ^{1}H at lower ℓ values and decreases as ℓ increases. Among the other light particles for ^{2}H, P_0 is also high at low ℓ and it tends to 0 for higher ℓ. Also for symmetric IMF, ^{24}Mg, it is very low at lower ℓ values and slightly increases as ℓ increases. Fig. 4.19 shows the penetration probability calculated at T=3.43 MeV, R=R_t+1 fm, relative to angular momentum values.

Fig.4.20 shows the summed cross section for light particles, intermediate mass fragments and total cross sections through the solid, dashed and dotted lines respectively. The value for σ_{LP} starts to contribute at ℓ=10 $\hbar$ and σ_{IMF} at ℓ=15 $\hbar$. Experimental summed cross sections is σ_{LP} =1065. 65 mb, σ_{IMF} =200 mb and σ_{tot} =1265mb. Our calculated cross section for σ_{LP}=1642.46 mb, σ_{IMF}=200 mb and σ_{tot}=1842.46 mb. As there is no fitting procedure is carried out this deviation is noted. If we change ΔR between the limits of 0.1 to 1.5 fm and we can arrive at exact values for cross section.

Table 4.1 Characteristic quantities for alpha decay of 34 even-even nuclei

$208 \leq A \leq 288$.

A	Z	Q value MeV	λs^{-1}	νs^{-1}	P_0	P_{tot}	Log_{10} $T_{1\2}$ (Cal)	Log_{10} $T_{1\2}$ (Exp)
208	84	5.22	3.48E-08	2.32E+21	3.49E-01	1.50E-29	7.30	6.18
210	84	5.41	4.64E-07	2.35E+21	3.59E-01	1.97E-28	6.17	7.08
212	86	6.38	3.06E-03	2.55E+21	3.91E-01	1.20E-24	2.36	3.16
218	84	6.11	2.30E-03	2.47E+21	3.96E-01	9.32E-25	2.48	2.27
220	86	6.40	5.13E-03	2.52E+21	3.87E-01	2.04E-24	2.13	1.75
222	86	5.59	6.19E-07	2.34E+21	3.39E-01	2.64E-28	6.05	5.52
222	88	6.68	9.13E-03	2.56E+21	3.77E-01	3.57E-24	1.88	1.53
224	88	5.79	6.75E-07	2.38E+21	3.28E-01	2.84E-28	6.01	5.50
224	90	7.30	3.46E-01	2.67E+21	3.89E-01	1.30E-22	0.302	0.021
226	88	4.87	2.51E-12	2.17E+21	2.89E-01	1.16E-33	11.4	11.7
226	90	6.45	1.19E-04	2.50E+21	3.40E-01	4.75E-26	3.77	1.49
228	90	5.52	2.31E-09	2.31E+21	2.97E-01	1.00E-30	8.48	6.78
230	90	4.77	3.91E-14	2.14E+21	2.70E-01	1.83E-35	13.2	13.4
230	92	5.99	8.47E-08	2.39E+21	2.99E-01	3.54E-29	6.9	6.24
230	94	7.18	2.36E-03	2.62E+21	3.32E-01	8.99E-25	2.47	2.01
232	92	5.41	5.20E-11	2.27E+21	2.77E-01	2.29E-32	10.1	16.6
234	92	4.86	1.28E-14	2.14E+21	2.58E-01	5.97E-36	13.7	12.9
236	92	4.57	1.05E-16	2.07E+21	2.49E-01	5.06E-38	15.8	13.9
238	94	5.59	6.43E-11	2.28E+21	2.67E-01	2.81E-32	10.0	10.4
240	94	5.26	5.81E-13	2.21E+21	2.56E-01	2.63E-34	12.1	11.3
240	96	6.40	1.35E-07	2.44E+21	2.80E-01	5.56E-29	6.71	6.37

242	94	4.98E	9.48E-15	2.14E+21	2.48E-01	4.42E-36	13.9	13.1
242	96	6.22	1.80E-08	2.39E+21	2.73E-01	7.53E-30	7.59	7.15
244	94	4.67	4.64E-17	2.07E+21	2.38E-01	2.25E-38	16.2	16.3
244	96	5.90	4.15E-10	2.32E+21	2.63E-01	1.79E-31	9.22	8.76
244	98	7.33	2.58E-04	2.59E+21	2.98E-01	9.96E-26	3.43	3.07
246	96	5.48	1.42E-12	2.23E+21	2.49E-01	6.35E-34	11.7	11.2
246	98	6.86	2.82E-06	2.50E+21	2.80E-01	1.13E-27	5.39	5.11
248	98	6.36	1.26E-08	2.40E+21	2.63E-01	5.26E-30	7.74	7.46
252	100	7.15	8.06E-06	2.53E+21	2.75E-01	3.19E-27	4.93	4.96
254	100	7.31	3.94E-05	2.55E+21	2.80E-01	1.55E-26	4.25	4.07
256	102	8.58	3.30E-01	2.75E+21	3.12E-01	1.20E-22	0.322	4.64
270	108	9.31	5.28E-01	2.81E+21	2.89E-01	1.88E-22	0.118	1.48
288	114	9.98	6.40E-01	2.84E+21	2.66E-01	2.25E-22	0.348	-0.12

Table 4.2 Characteristic quantities for alpha decay of 40 even-odd nuclei

$210 \leq A \leq 290$

A	Z	Q value MeV	λ_S^{-1}	ν_S^{-1}	P_0	P_{Tot}	$\log_{10}T_{1/2}$ (Cal)	$\log_{10}T_{1/2}$ (exp)
210	83	5.04E	1.18E-08	2.27E+21	3.50E-01	5.21E-30	7.77	14.0
212	85	7.82E	2.38E+03	2.82E+21	5.52E-01	8.44E-19	-3.54	-0.50
212	91	8.43	5.29E+02	2.93E+21	4.59E-01	1.81E-19	-2.88	-2.10
214	87	8.59	8.22E+04	2.94E+21	6.07E-01	2.79E-17	-5.07	-2.30
214	91	8.28	1.95E+02	2.89E+21	4.47E-01	6.75E-20	-2.45	-1.77
216	85	7.95	7.03E+03	2.82E+21	5.65E-01	2.49E-18	-4.01	-3.52
216	87	9.18	4.13E+06	3.03E+21	7.74E-01	1.36E-15	-6.78	-8.15
216	89	9.24	8.89E+05	3.04E+21	6.48E-01	2.92E-16	-6.11	-3.36
218	85	6.87	1.25E+00	2.62E+21	4.39E-01	4.76E-22	-0.254	0.18
218	87	8.01	1.68E+03	2.82E+21	5.14E-01	5.97E-19	-3.39E	-3.00
218	89	9.37	2.24E+06	3.05E+21	6.82E-01	7.35E-16	-6.51	-5.97
218	91	9.82	5.07E+06	3.13E+21	6.78E-01	1.62E-15	-6.86	-3.95
220	87	6.80	8.03E-02	2.59E+21	4.00E-01	3.10E-23	0.936	1.44
220	89	8.35	2.94E+03	2.87E+21	5.01E-01	1.02E-18	-3.63	-1.58
220	91	9.83	6.14E+06	3.12E+21	6.83E-01	1.97E-15	-6.95	-8.11
222	91	8.86	1.57E+04	2.95E+21	5.08E-01	5.32E-18	-4.35	-2.49
224	91	7.69	3.43E+00	2.74E+21	4.01E-01	1.25E-21	-0.694	-0.07
226	93	8.20	2.65E+01	2.82E+21	4.05E-01	9.39E-21	-1.58	-1.45
246	101	8.89	5.31E+00	2.84E+21	3.38E-01	1.87E-21	-0.884	-0.035
254	99	6.62	9.34E-08	2.43E+21	2.63E-01	3.85E-29	6.87	7.38
258	101	7.27	1.15E-05	2.53E+21	2.70E-01	4.54E-27	4.78	6.65

260	107	1.05	1.62E+03	3.02E+21	3.50E-01	5.35E-19	-3.37	-1.39
266	107	9.56	6.31E+00	2.87E+21	3.07E-01	2.20E-21	-0.960	0.40
266	109	1.10	8.93E+03	3.07E+21	3.55E-01	2.91E-18	-4.11	-2.22
268	109	1.07	2.04E+03	3.03E+21	3.41E-01	6.73E-19	-3.47	0.152
270	107	9.30	1.19E+00	2.81E+21	2.96E-01	4.22E-22	-0.233	7.00
270	109	1.03	2.27E+02	2.97E+21	3.23E-01	7.66E-20	-2.52	-2.22
272	107	9.31	1.39E+00	2.80E+21	2.96E-01	4.96E-22	-0.3.03	0.944
272	111	1.14	2.80E+04	3.11E+21	3.56E-01	8.99E-18	-4.61	-0.041
274	107	8.50	3.13E-03	2.67E+21	2.67E-01	1.17E-24	2.35	6.95
274	111	1.16	7.10E+04	3.12E+21	3.65E-01	2.27E-17	-5.01	-1.54
276	109	9.80	8.30E+00	2.86E+21	2.99E-01	2.90E-21	-1.08E	-1.40
278	109	9.11	6.84E-02	2.75E+21	2.73E-01	2.48E-23	1.01E	1.46
278	111	1.07	5.68E+02	2.99E+21	3.20E-01	1.90E-19	-2.91	-0.194
280	111	9.99	6.30E+00	2.87E+21	2.89E-01	2.19E-21	-9.58	-0.194
282	111	9.38	9.91E-02	2.78E+21	2.68E-01	3.57E-23	8.45	0.580
284	113	1.02	7.65E+00	2.90E+21	2.83E-01	2.64E-21	-1.04	0.279
286	113	9.69	1.87E-01	2.81E+21	2.64E-01	6.67E-23	0.568	0.0042
288	115	1.10	1.94E+02	2.99E+21	2.96E-01	6.49E-20	-2.45	1.85
290	115	1.03	2.52E+00	2.88E+21	2.70E-01	8.76E-22	-0.561	-0.721

Table 4.3 Characteristic quantities for alpha decay of 47 odd-even nuclei

$211 \leq A \leq 289$.

A	Z	Q MeV	λ_S^{-1}	ν_S^{-1}	P_0	P_{tot}	$Log_{10}T_{1\backslash 2}$ (cal)	$log_{10}T_{1\backslash 2}$ (E)
211	84	7.59	1.10E+03	2.78E+21	5.51E-01	3.95E-19	-3.20	1.40
213	84	8.54	1.05E+06	2.94E+21	7.82E-01	3.56E-16	-6.18	-4.50
213	86	8.24	1.94E+04	2.89E+21	5.84E-01	6.71E-18	-4.45	-0.71
215	86	8.84	1.18E+06	2.98E+21	7.25E-01	3.96E-16	-6.23	-5.64
215	88	8.87	2.06E+05	2.99E+21	6.17E-01	6.90E-17	-5.47	-1.99
215	90	7.67	5.20E+00	2.78E+21	4.17E-01	1.87E-21	-0.875	0.08
217	84	6.66	5.00E-01	2.58E+21	4.38E-01	1.94E-22	0.142	0.180
217	86	7.89E	1.71E+03	2.81E+21	5.25E-01	6.10E-19	-3.39	-3.27
217	88	9.16	1.47E+06	3.02E+21	6.86E-01	4.87E-16	-6.33	-5.79
219	86	6.95	8.48E-01	2.62E+21	4.27E-01	3.23E-22	-0.0875	0.598
219	88	8.14	1.64E+03	2.84E+21	5.02E-01	5.76E-19	-3.37	-2.00
219	90	9.51	2.16E+06	3.07E+21	6.58E-01	7.04E-16	-6.49	-5.98
219	92	9.86	2.79E+06	3.13E+21	6.30E-01	8.93E-16	-6.61	-4.26
221	88	6.88	5.93E-02	2.60E+21	3.91E-01	2.28E-23	1.07	1.45
221	90	8.63	8.11E+03	2.92E+21	5.07E-01	2.78E-18	-4.07	-2.77
223	88	5.98	5.98E-06	2.42E+21	3.38E-01	2.47E-27	5.06	5.99
223	90	7.57	3.22E+00	2.72E+21	4.08E-01	1.18E-21	-0.667	-0.222
223	92	8.95	1.16E+04	2.96E+21	4.92E-01	3.91E-18	-4.22	-4.68
225	92	8.01	1.68E+01	2.79E+21	4.08E-01	6.03E-21	-1.39	-1.21
227	90	6.15	4.54E-06	2.44E+21	3.24E-01	1.86E-27	5.18	8.84
229	90	5.17	1.78E-11	2.23E+21	2.84E-01	8.01E-33	10.6	10.4
235	92	4.68	6.46E-16	2.10E+21	2.53E-01	3.08E-37	15.0	16.3

239	94	5.24	4.74E-13	2.21E+21	2.56E-01	2.15E-34	12.2	10.9
243	96	6.17E	1.07E-08	2.38E+21	2.71E-01	4.52E-30	7.81	13.0
245	96	5.62E	1.08E-11	2.27E+21	2.54E-01	4.78E-33	10.8	11.4
247	96	5.35	2.51E-13	2.20E+21	2.45E-01	1.14E-34	12.4	14.7
247	100	8.21	7.99E-02	2.73E+21	3.16E-01	2.93E-23	9.38	0.708
249	98	6.30	6.13E-09	2.38E+21	2.61E-01	2.57E-30	8.05	10.0
251	98	6.18	1.58E-09	2.35E+21	2.57E-01	6.73E-31	8.64	11.5
251	102	8.91	3.02E+00	2.83E+21	3.28E-01	1.07E-21	-0.639	0.008
255	104	9.07	1.85E+00	2.83E+21	3.15E-01	6.52E-22	-0.426	10^{-3}
257	100	6.86	5.10E-07	2.46E+21	2.64E-01	2.07E-28	6.13	6.94
257	104	9.04	1.62E+00	2.82E+21	3.13E-01	5.73E-22	-0.368	0.633
265	108	10.06	1.77E+03	3.02E+21	3.45E-01	5.86E-19	-3.41	-2.77
267	110	12.3	3.39E+06	3.24E+21	4.25E-01	1.04E-15	-6.69	-5.00
269	108	9.63	4.74E+00	2.86E+21	3.01E-01	1.66E-21	-0.835	1.43
269	110	11.6	1.14E+05	3.14E+21	3.77E-01	3.63E-17	-5.22	-3.64
271	110	10.9	2.48E+03	3.04E+21	3.37E-01	8.16E-19	-3.55	-1.05
273	110	11.4	4.29E+04	3.10E+21	3.64E-01	1.39E-17	-4.79	-0.921
275	108	9.20	2.89E-01	2.78E+21	2.84E-01	1.04E-22	0.380	-0.538
277	112	11.6	3.92E+04	3.11E+21	3.53E-01	1.26E-17	-4.75	-3.00
281	110	8.96	9.94E-03	2.72E+21	2.61E-01	3.66E-24	1.84	-0.0223
281	112	10.3	2.03E+01	2.91E+21	2.93E-01	6.96E-21	-1.47	-0.0132
285	112	8.80	5.29E-04	2.68E+21	2.44E-01	1.97E-25	3.12	-1.49
285	114	11.0	3.59E+02	3.00E+21	3.04E-01	1.20E-19	-2.71	-0.328
287	114	10.4	1.26E+01	2.91E+21	2.82E-01	4.33E-21	-1.26	-0.284
289	114	9.85	2.73E-01	2.82E+21	2.62E-01	9.67E-23	0.405	0.380

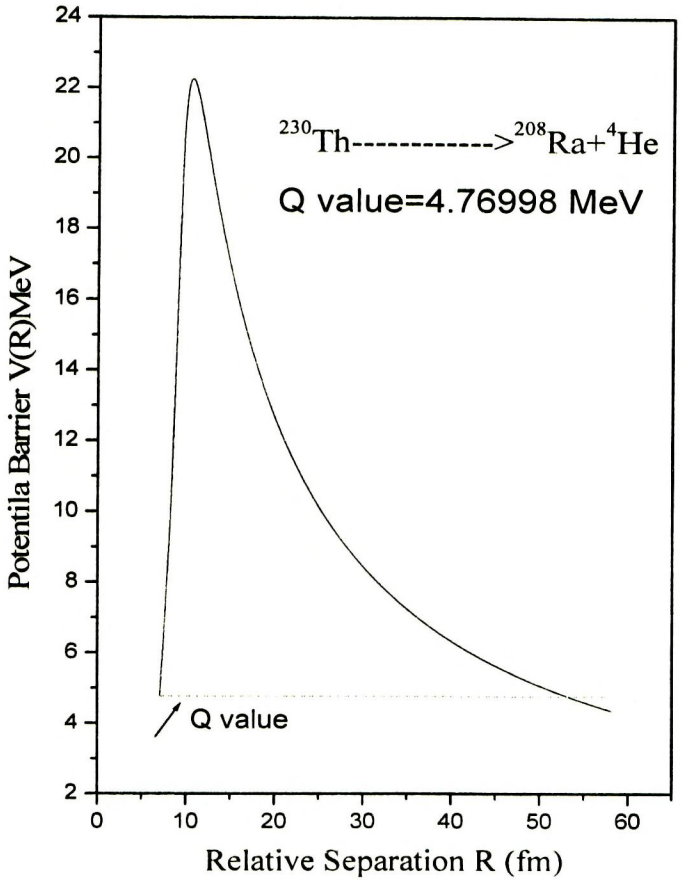

Fig.4.1

Potential Barrier for the parent nucleus ^{230}Th for alpha decay.

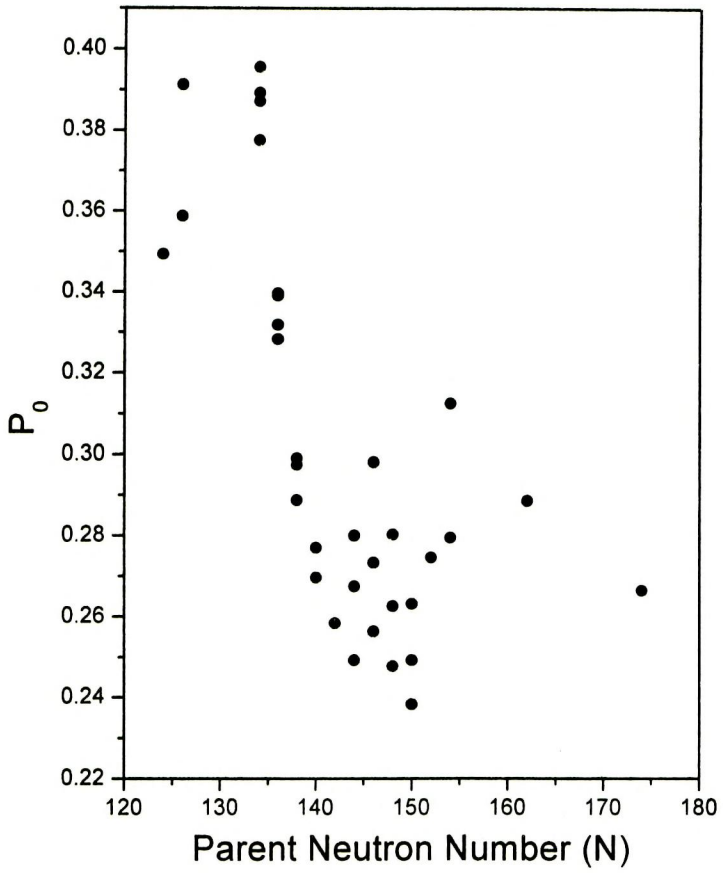

Fig. 4.2

Preformation probability of 34 even-even nuclei with respect to the parent Neutron Number N

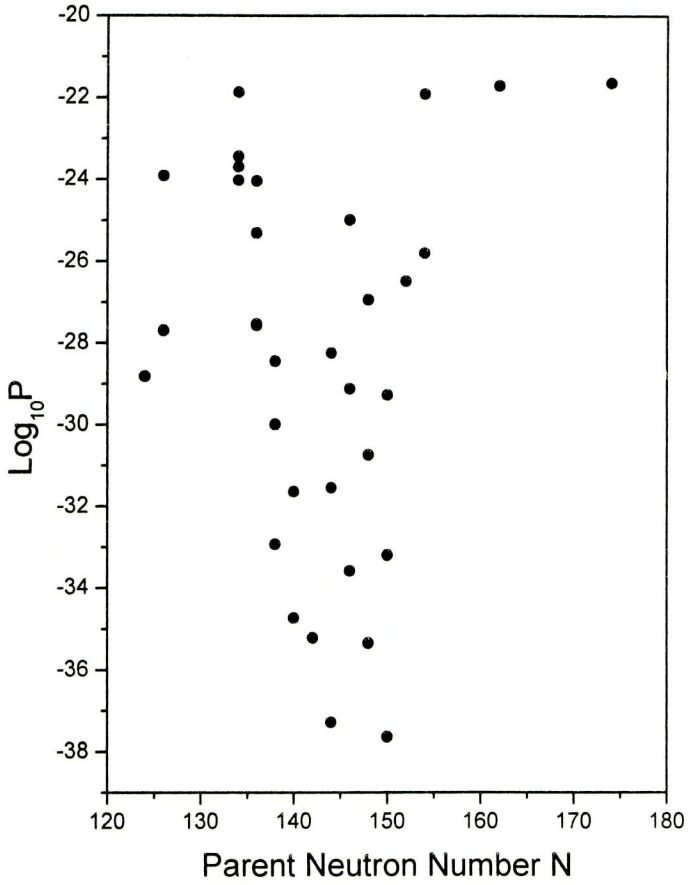

Fig .4.3

Calculated decimal logarithmic values of penetrability values for 34 even-even nuclei relative to parent neutron number N.

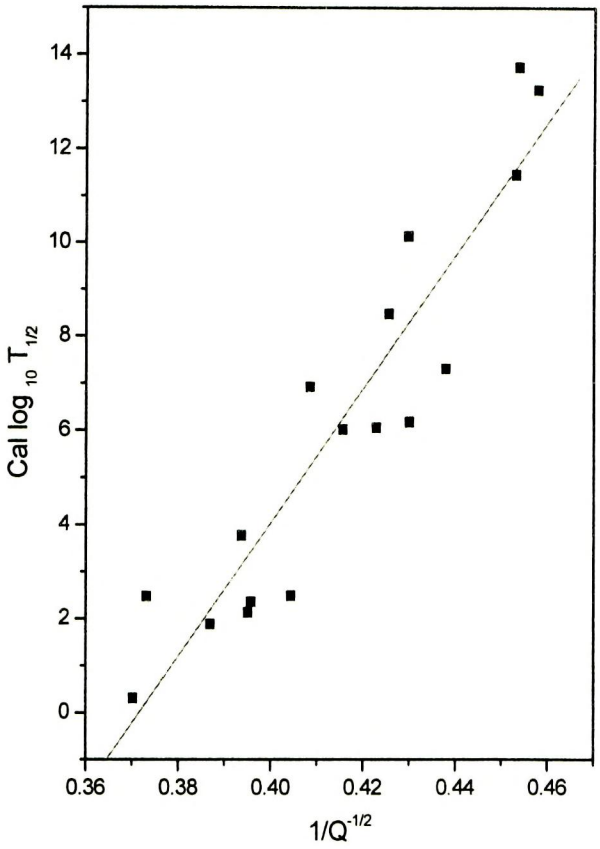

Fig .4.4 (a)

Calculated log $T_{1/2}$ values relative to $\frac{1}{\sqrt{Q}}$ for 34 even- even nuclei.

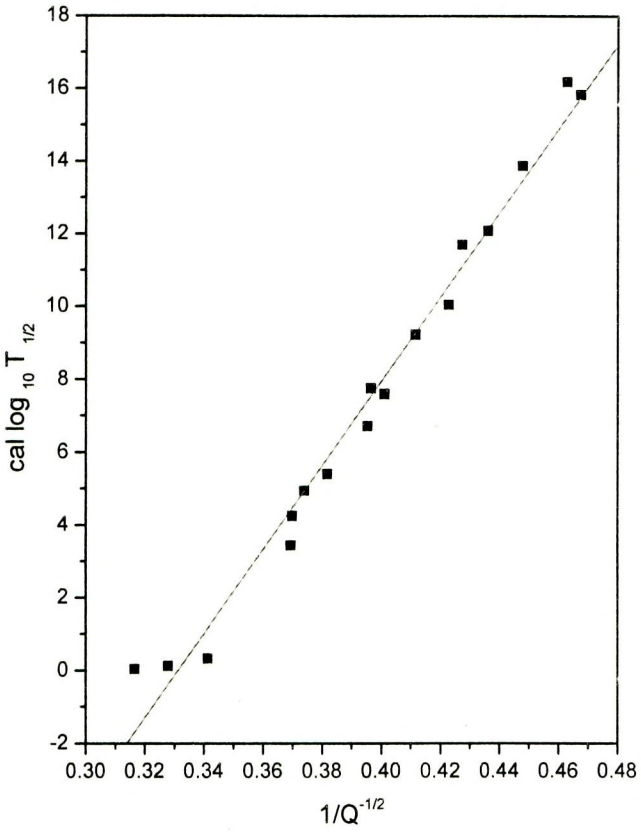

Fig .4.4 (b)

Calculated log $T_{1/2}$ values relative to $\frac{1}{\sqrt{Q}}$ for 34 even-even nuclei

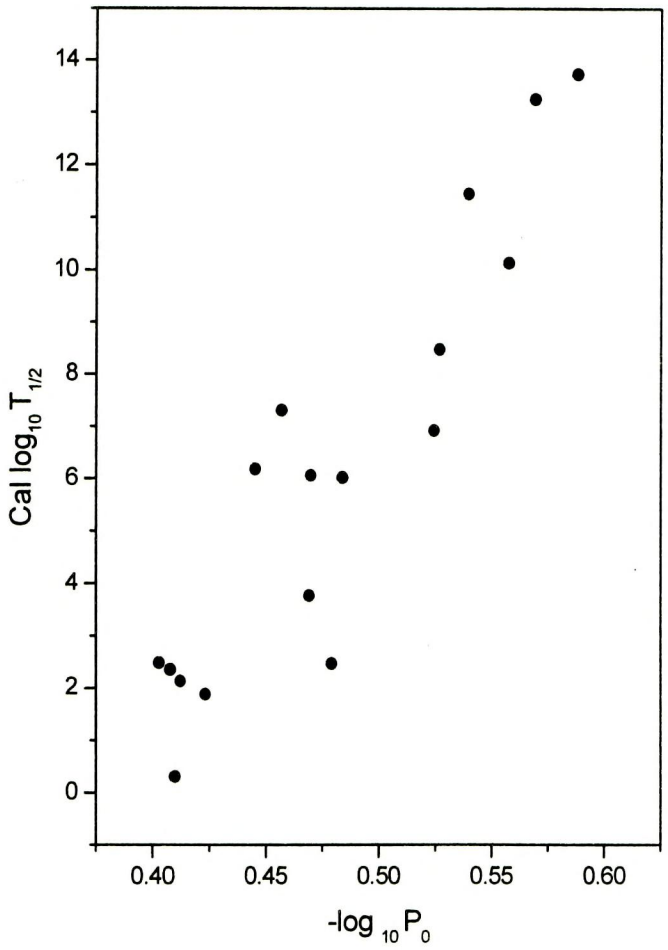

Fig .4.5 (a)

Calculated $\log_{10}T_{1/2}$ against $-\log_{10}P_0$ for neutron around 126

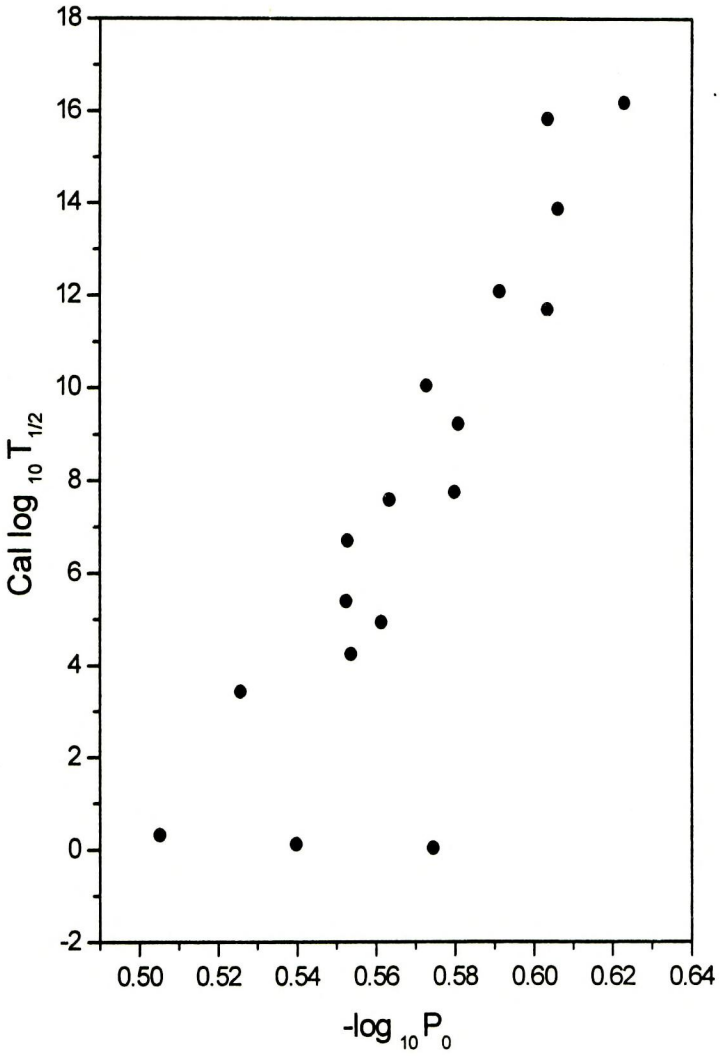

Fig. 4.5(b)

Calculate $\log_{10}T_{1/2}$ against $-\log_{10}P_0$ for neutron around 152

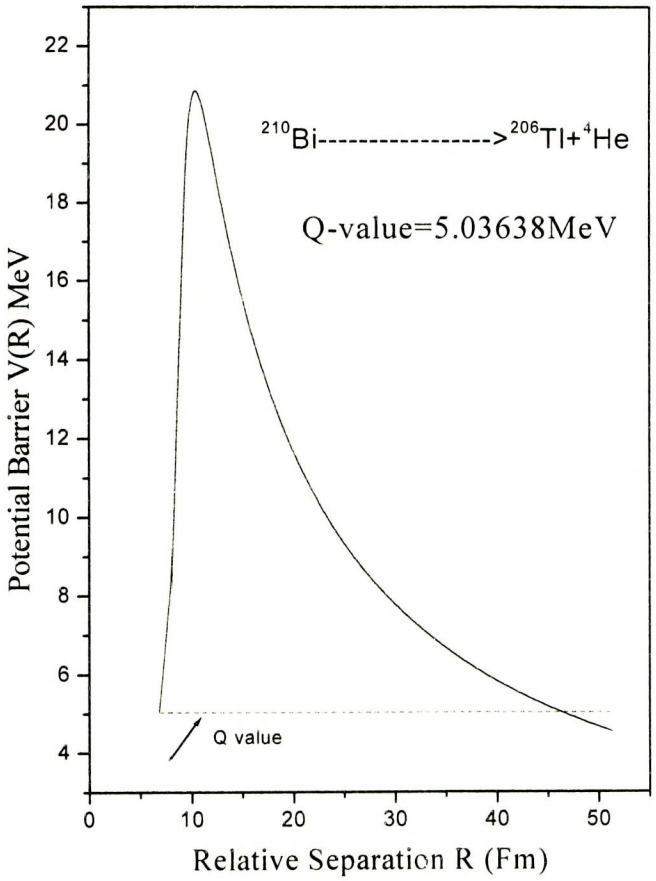

Fig. 4.6

Potential Barrier for the parent nucleus ^{210}Bi for alpha decay.

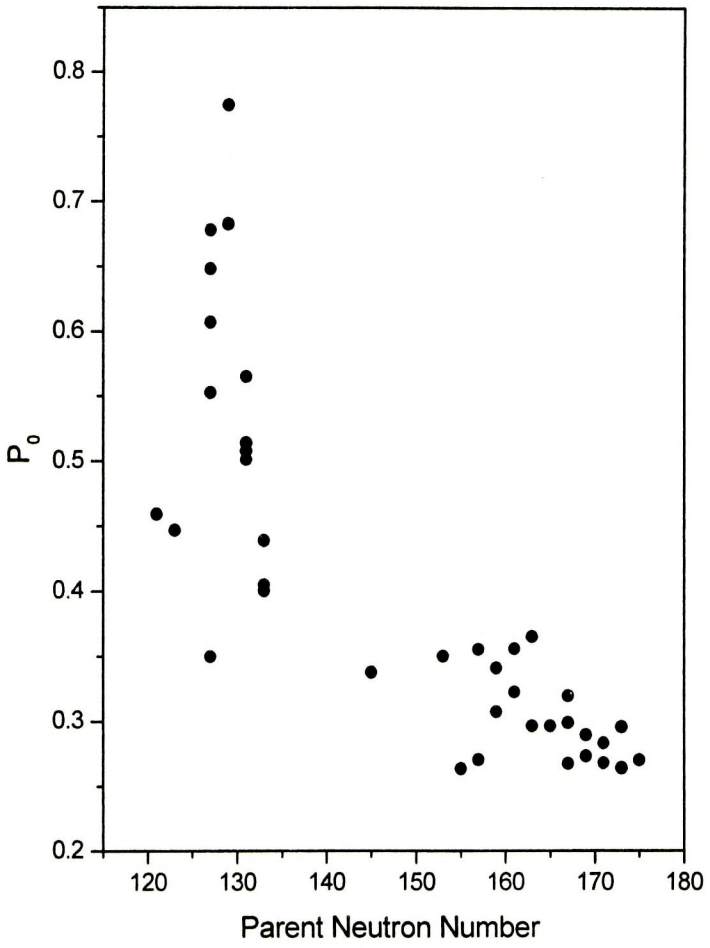

Fig .4.7

Preformation probability of 40 even odd nuclei with respect to the parent Neutron Number N

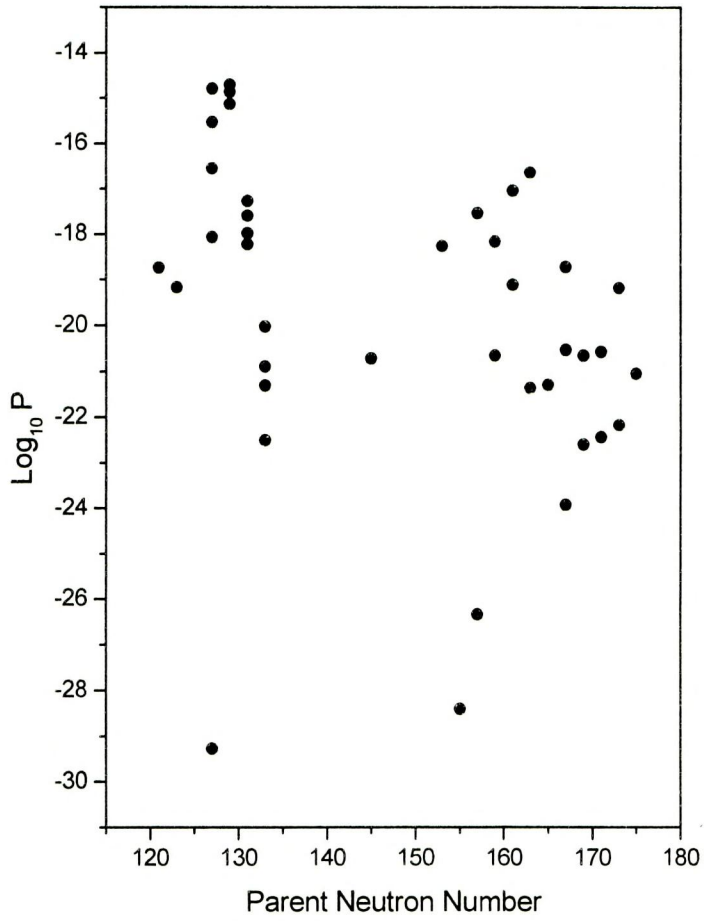

Fig. 4.8

Calculated decimal logarithmic values of penetrability values relative to parent neutron number N, for 40 even-odd nuclei.

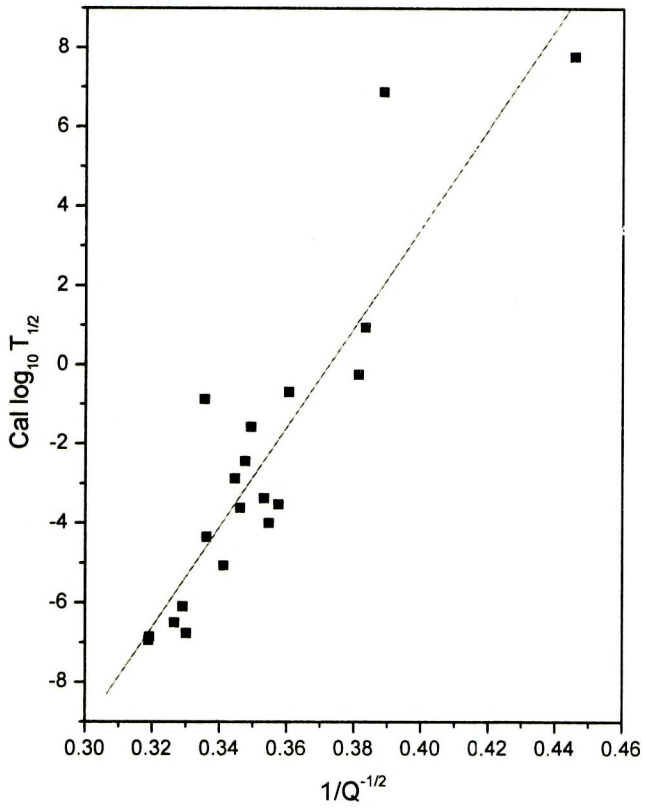

Fig.4.9 (a)

Calculated log $T_{1/2}$ values relative to $\frac{1}{\sqrt{Q}}$ for 40 even odd nuclei.

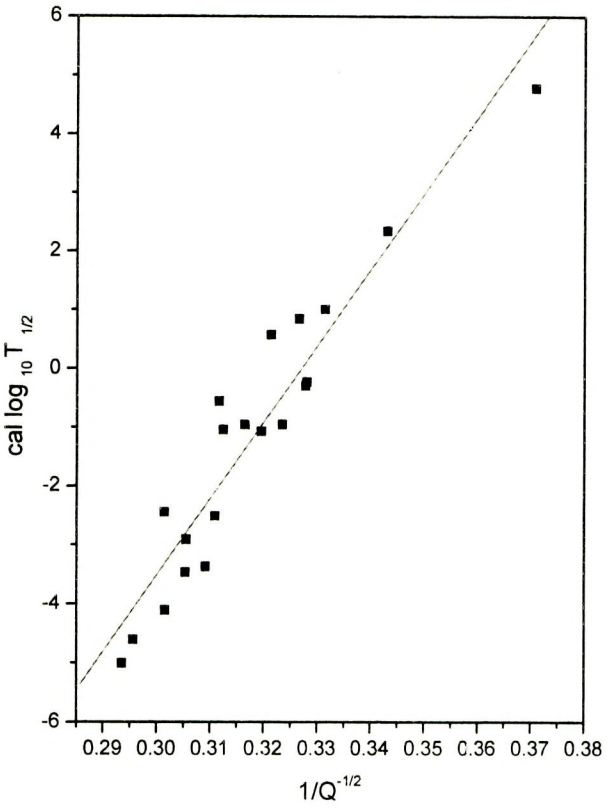

Fig .4.9 (b)

Calculated log $T_{1/2}$ values relative to $\frac{1}{\sqrt{Q}}$ for 40 even odd nuclei.

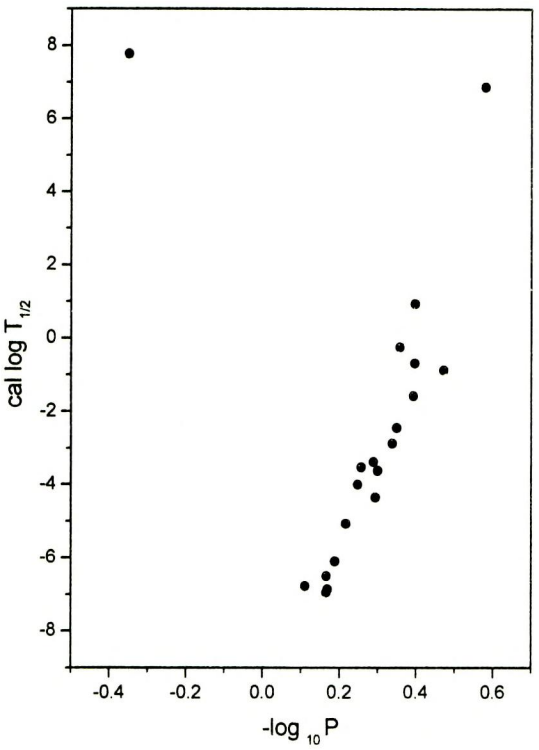

Fig. 4.10 (a)

Calculated $\log_{10} T_{1/2}$ against $-\log_{10} P_0$ for around N=126

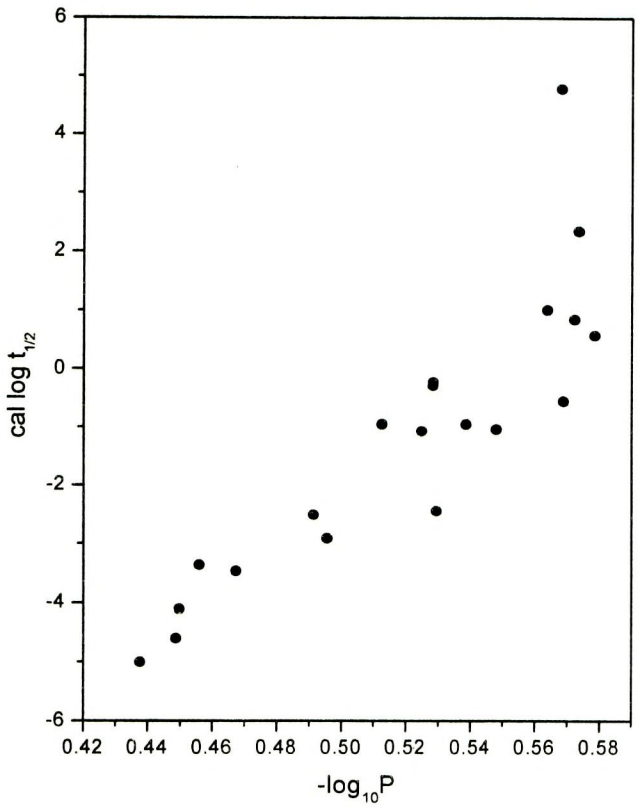

Fig .4.10 (b)

Calculated $\log_{10}T_{1/2}$ against $-\log_{10}P_0$ for around N=152

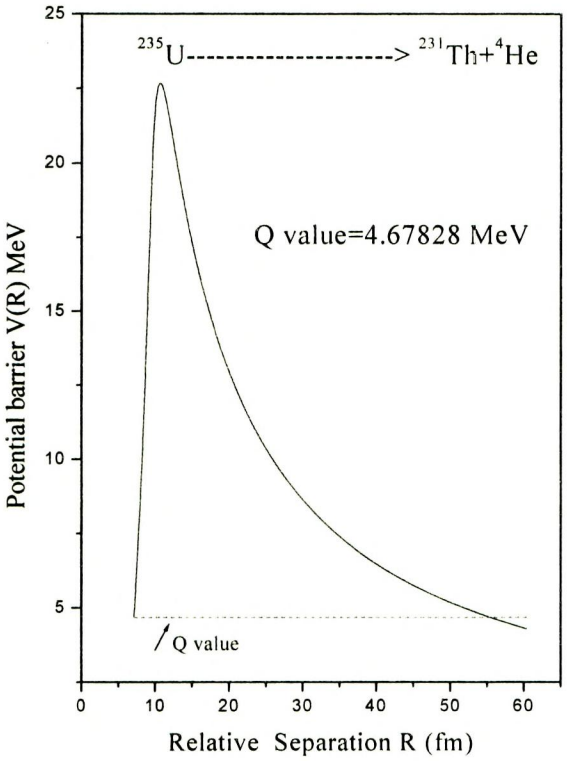

Fig .4.11

Potential barrier for the parent nucleus ^{235}U for alpha decay.

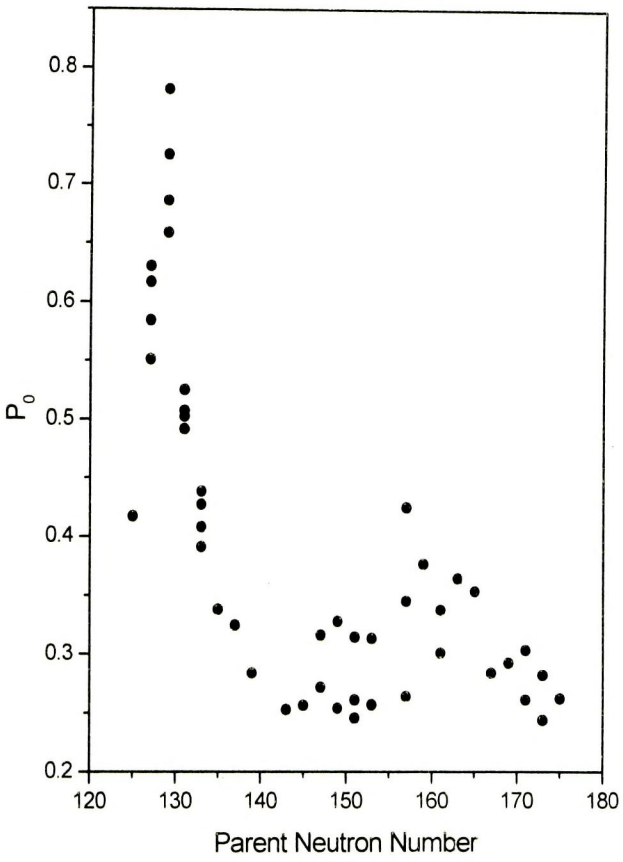

Fig .4.12

Preformation probability of 47 odd-even nuclei with respect to the parent Neutron Number N

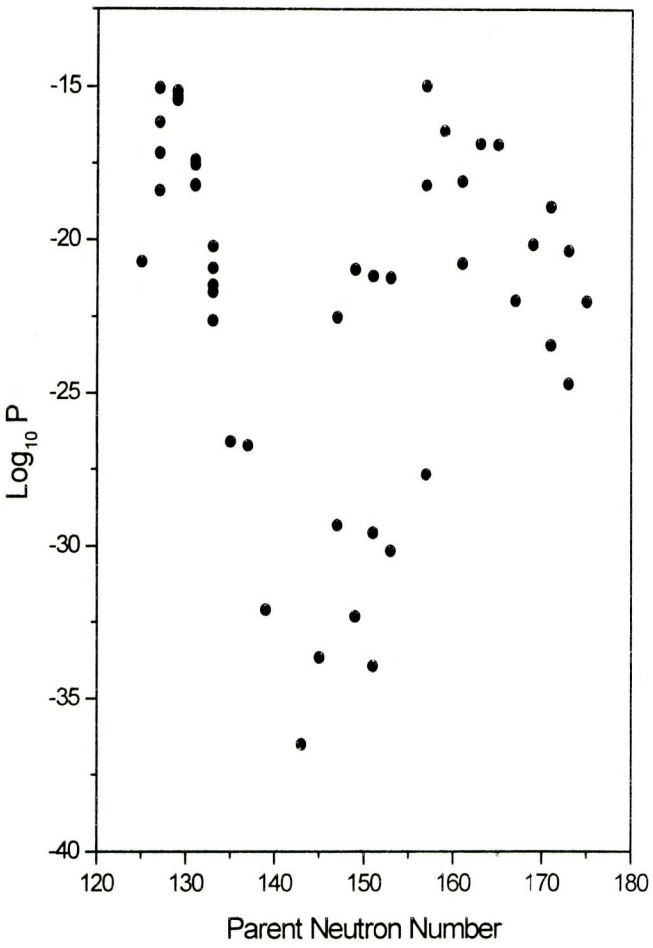

Fig. 4.13

Calculated decimal logarithmic values of penetrability values relative to parent neutron number (N) of 47 odd-even nuclei

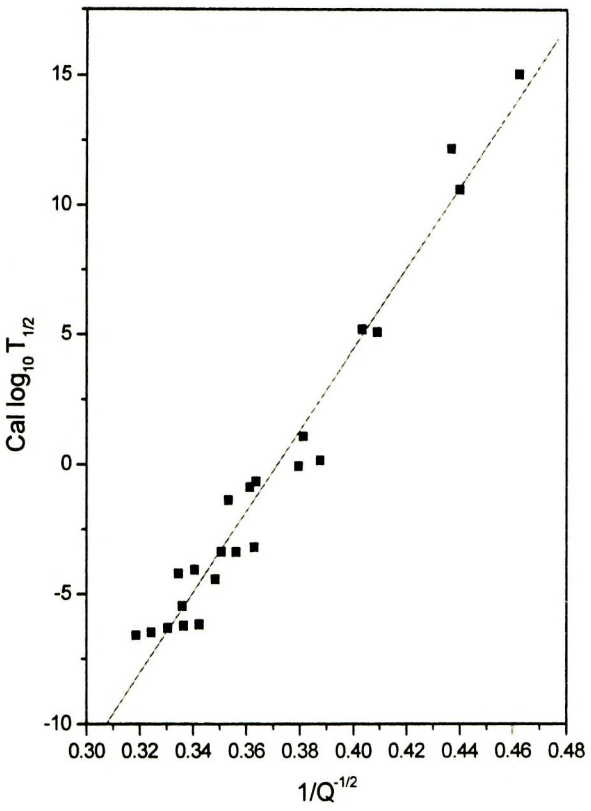

Fig 4.14 (a)

Calculated $\log_{10} T_{1/2}$ values relative to $\frac{1}{\sqrt{Q}}$ for 47 odd-even nuclei around

Neutron number N= 126

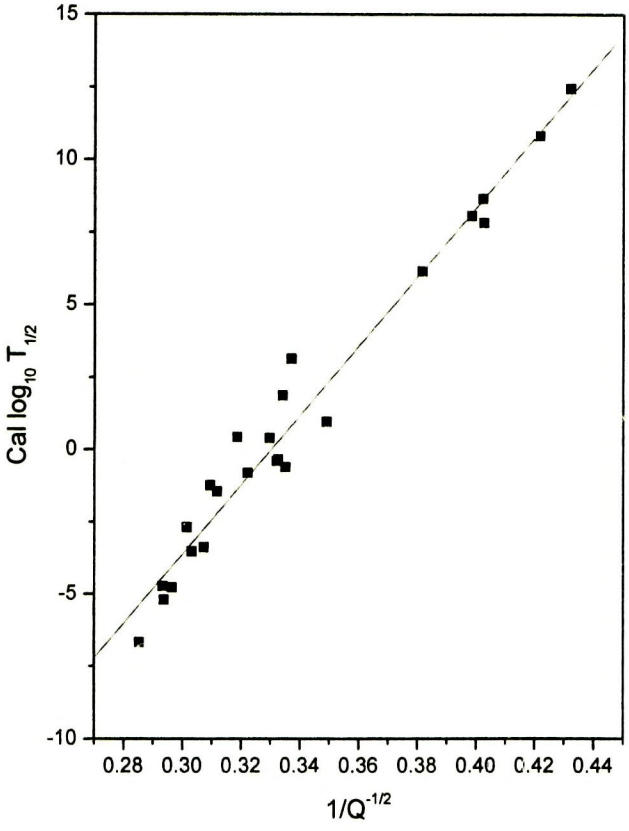

Fig 4.14 (b)

Calculated log $T_{1/2}$ values relative to $\frac{1}{\sqrt{Q}}$ for 47odd-even nuclei, around neutron number N=152.

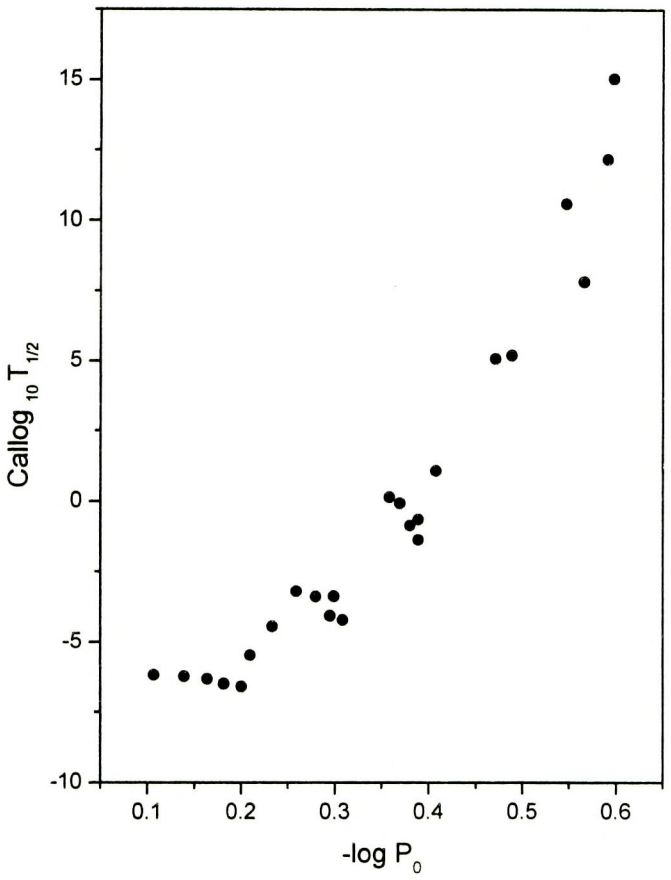

Fig.4. 15 (a)

Calculate $\log_{10}T_{1/2}$ against $-\log_{10}P_0$

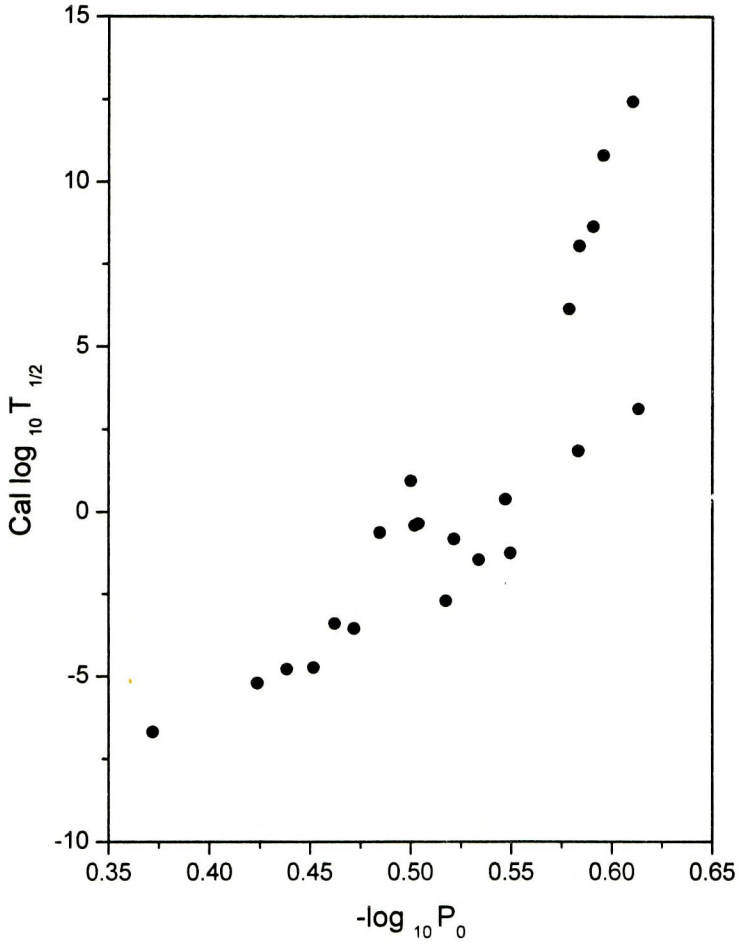

Fig .4.15(b)

Calculate $\log_{10}T_{1/2}$ against $-\log_{10}P_0$

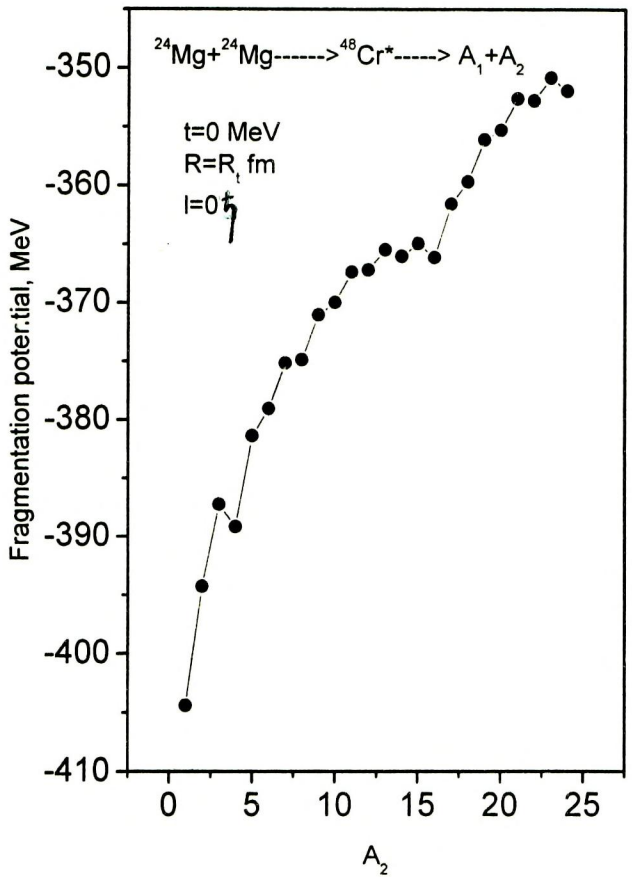

Fig. 4.16

Fragmentation potential for the decay of hot and rotating $^{48}Cr^*$ formed in $^{24}Mg+^{24}Mg$ reaction

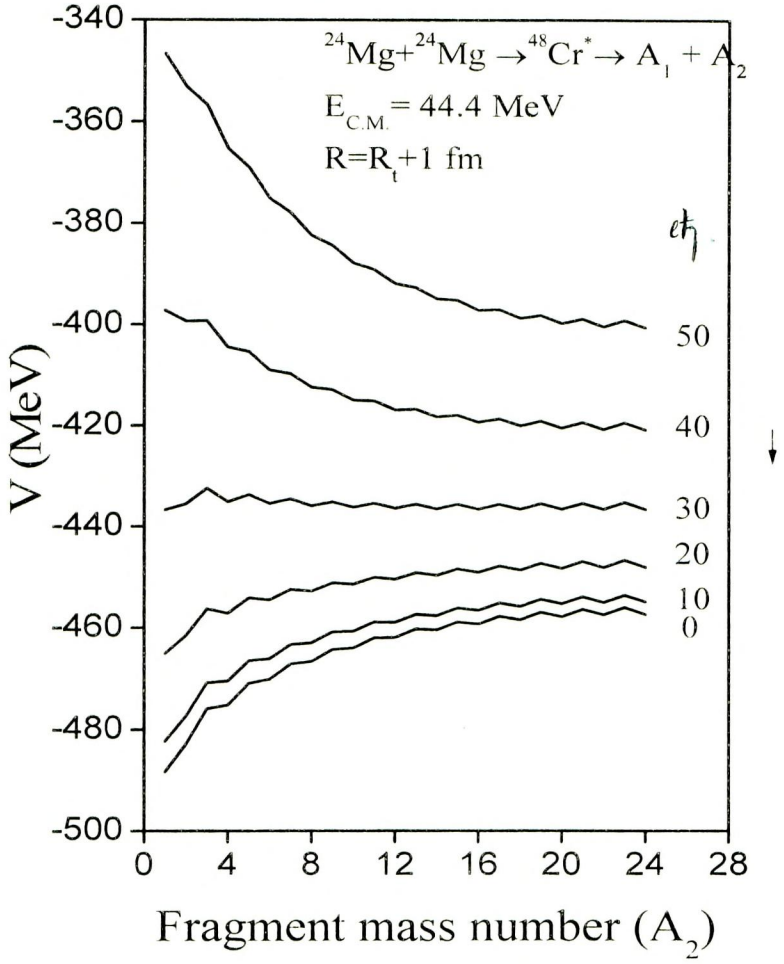

Fig.4.17

Fragmentation potential at T=3.43 MeV with R=Rt+1 fm for different angular momentum values.

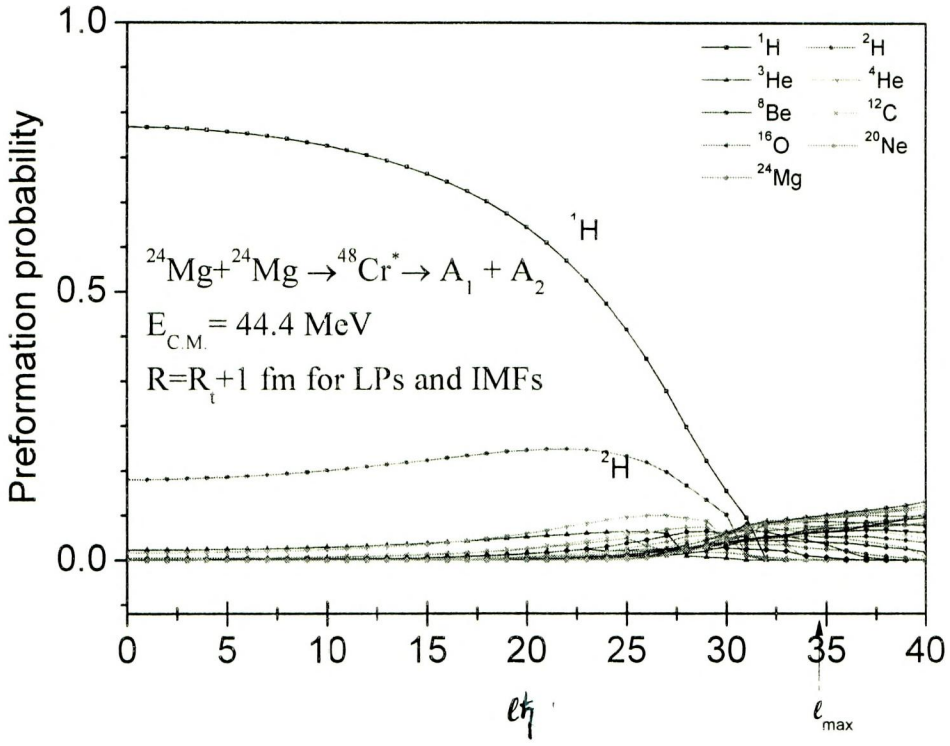

Fig. 4.18

The fragment preformation probability (P_0) as a function of angular momentum $l\hbar$ for the ^{48}Cr*compound system is calculated by Guet *et al.*'s formula at T= 3.43 MeV and $E_{c.m.}$ = 44.4 MeV.

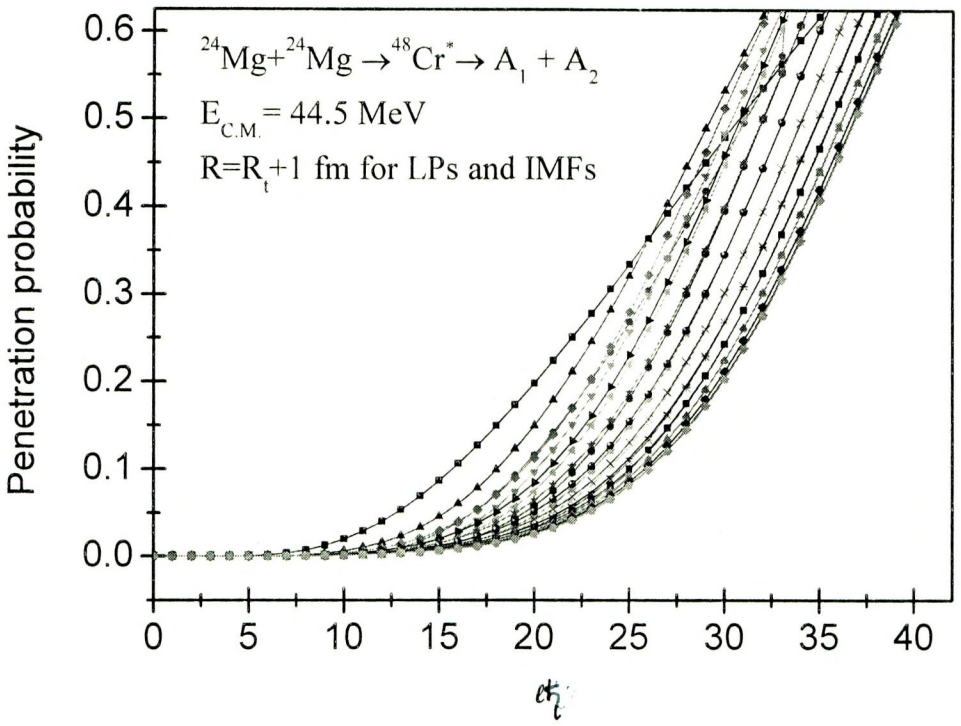

Fig.4.19

The fragment penetration probability P asa function of angular momentum l for the ^{48}Cr* compound system is calculated Guet *et al.*'s formula at T = 3.43 MeV and $E_{c.m.}$ = 44.4 MeV.

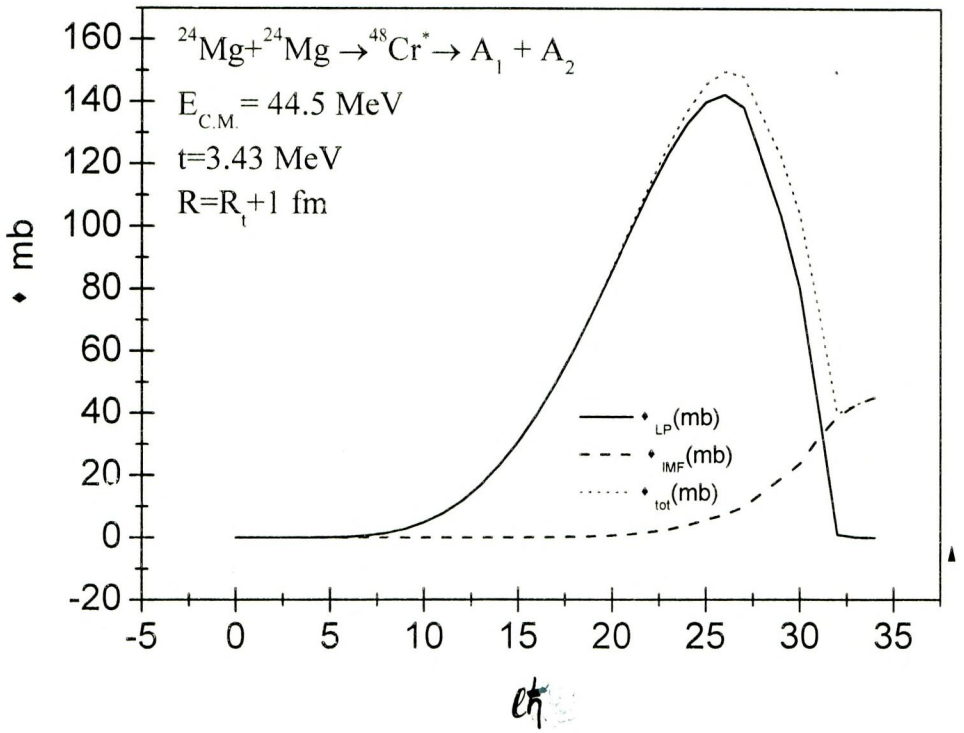

Fig 4.20

Light particle cross sections σ_{LP} (solid line), intermediate mass fragment cross sections σ_{IMF} (dashed line), and their sum σ_{Total} (dotted line) calculated for $^{48}Cr^{*}$at fitted T=3.43 MeV using Guet *et al.*'s formula.